

# DYNAMIC STIFFNESS CALCULATION OF A ROTOR-BEARING SYSTEM WITH AN ELECTRO-MAGNETIC ACTUATOR AS EXCITATION SOURCE

Helio Fiori de Castro, heliofc@fem.unicamp.br

Katia Lucchesi Cavalca, katia@fem.unicamp.br

Laboratory of Rotating Machinery – Mechanical Engineering Faculty – University of Campinas

**Abstract.** *Important parameters in the rotating machine model, as the dynamic stiffness of the rotating system supported by journal bearings, can be determined through the dynamic system response to an excitation force (synchronous or nonsynchronous). The dynamic stiffness has direct relation with the phenomenon of fluid-induced instability, generally associated to hydrodynamic bearings of fixed geometry, because it allows to determine the imminence of the instable motion. This kind of instable motion occurs due to precessional orbits in the rotor-bearing system. This instability is called “oil whirl” or “oil whip”. The oil whirl phenomenon occurs when the journal bearings are lightly loaded and the shaft is whirling at a frequency close to one-half of rotor angular speed. When the rotation speed of the rotor reaches approximately twice the natural frequency (first critical speed) the oil whip phenomenon occurs and remains even if the rotor rotation speed increases. Its frequency and vibration mode corresponds to the first critical speed. The nonlinear motion due to the fluid-induced instabilities can be very harmful to the system, especially the oil whip phenomenon, what confirms the necessity to foresee the threshold of the instable motion. Therefore, the dynamic stiffness, which is defined as the machine's measure of resistance to instability, can be an important parameter to preview this dynamic behaviour. This research proposes the modeling and experimental analysis of a flexible rotor with a central disc, assuming unbalance excitation. A nonlinear hydrodynamic force model is considered for short bearing and laminar flow, so that it is possible to simulate the rotor-bearing system under fluid-induced instability. Experimental results are obtained in an experimental test rig. The source of non-synchronous excitation is an electro-magnetic actuator, which means a non-contact excitation. This research presents a contribution for the rotating machine design area, as it intends to verify the consistence of nonlinear rotor-bearing model and its behaviour under instable situation, introducing the system dynamic stiffness as a controlled parameter in instability control.*

**Keywords:** *fluid-induced instability, journal bearing, dynamic stiffness, electro-magnetic actuator, rotor dynamic.*

## 1. INTRODUCTION

The interaction between the rotating system and the oil film in a hydrodynamic bearing causes instable dynamic behaviour (see Gash *et al.*, 2002, and Muszynska and Bently, 1989), which is characterized by a sub-synchronous forward precessional vibration. This behaviour is known as oil whirl and oil whip and was discovered by Newkirk (1924, 1925) and analysed by Lund and Saibel (1967), Muszynska (1986 and 1988), Crandall (1990), Childs (1993), Gasch *et al.* (2002) and Castro *et al.* (2006 and 2008).

The fluid-induced instabilities are known as self-exciting vibration of a rotor-bearing system. Due to oil whirl, the shaft vibrates in a frequency close to half of the rotation speed. When the rotation speed reaches twice the first natural frequency, the oil whip instability starts, which can be severally harmful for the rotor-bearing system. In this case, the vibration frequency (or self-excitation frequency) is equal to the first natural frequency.

In order to estimate the instability threshold, Muszynska and Bently (1990) proposed the calculation of the rotor-bearing system dynamic stiffness, through a non-synchronous excitation. In that case, the system presents an instable motion when the real and the imaginary parts of the dynamics stiffness are simultaneously null.

On the other hand, mathematical models were developed, in order to represent real machines with considerable confidence. Therefore, several researches were performed to determine better models for rotating machinery such as turbo generators and multi stage pumps, which are horizontal rotating machines of high load capacity. Some of these numerical simulations were developed to study cylindrical hydrodynamic bearings by Capone (1986 and 1991), where the orbits of the shaft in the bearings were obtained, considering a nonlinear hydrodynamic force model.

Castro *et al.* (2006) considered this nonlinear hydrodynamic journal bearing model to simulate fluid-induced instabilities (oil whirl and oil whip), verifying that this model can numerically represent the dynamic behaviour of a rotor under fluid-induced instabilities. After that, Castro *et al.* (2008) analysed the nonlinear aspect of this simulation and compared it to experimental results.

Afterwards, the authors applied the concept of dynamic stiffness (see Bently *et al.*, 1998, and Muszynska and Bently, 1990) to analyse fluid-induced instability considering nonlinear effects. This research proposes the modelling and analysis of a flexible rotor with a central disc, assuming unbalanced excitation. Besides, an experimental analysis is also accomplished. For simulation purpose, a finite element model and a nonlinear hydrodynamic force model are considered, so that it is possible to simulate the rotor-bearing system under fluid-induced instability. An experimental

test rig was used for the tests. The source of non-synchronous excitation is an electro-magnetic actuator, which means a non-contact excitation.

## 2. ROTOR-BEARING SYSTEM NONLINEAR MODEL

The mathematical model (adopted in this work) of a rotating system can be divided into two parts: the finite element model of the shaft and the concentrated mass to the disk (see Archer, 1965, Ruhl and Booker, 1972, and Nelson and McVaugh, 1976), and the nonlinear hydrodynamic supporting forces (Capone, 1986 and 1991) of the cylindrical journal bearing, which is obtained by the Reynolds' equation solution for short bearings.

Equation (1) describes the pressure distribution inside the cylindrical journal bearing (Fig. 1.a), based on the Reynolds' equation solution for laminar flux condition (Reynolds, 1886). This expression considers the dimensionless oil film thickness  $h$  and the dimensionless axial length  $z$  (Fig. 1.a), due to the losses of lubricating fluid in short journal bearing. The bearing parameters are radial clearance  $C$ , bearing length  $L$ , bearing radius  $R$  and oil viscosity  $\mu$  and the rotation speed is  $\Omega$ .

$$\frac{\partial}{\partial v} \left( h^3 \frac{\partial p}{\partial v} \right) + k^2 \frac{\partial}{\partial z} \left( \frac{h^3}{\mu} \frac{\partial p}{\partial z} \right) = \frac{\partial h}{\partial v} + 2 \frac{dh}{d\tau} \quad (1)$$

The solution of Eq. (1) considers the axial gradient  $\frac{\partial p}{\partial z}$  due to axial losses of lubricating fluid in a short journal bearing, neglecting the pressure gradient in the angular direction  $\frac{\partial p}{\partial v}$  (Childs, 1993). Therefore, the result of the differential equation with this simplification is:

$$p(v, z) = \frac{1}{2} \left( \frac{L}{D} \right)^2 \left[ \frac{(x-2\dot{y})\sin(v) - (y+2\dot{x})\cos(v)}{(1-x\cos(v) - y\sin(v))^3} \right] (4z^2 - 1) \quad (2)$$

In order to determine the force generated by the oil film pressure distribution, the shaft contact area,  $dA = R \cdot dv \cdot L \cdot dz$ , is considered in Eq. (3):

$$Fh = \begin{cases} Fh_x \\ Fh_y \end{cases} = -\mu\Omega \left( \frac{R^2}{C^2} \right) \left( \frac{L^2}{D^2} \right) (R.L) \frac{[(x-2\dot{y})^2 + (y+2\dot{x})^2]^{\frac{1}{2}}}{(1-x^2-y^2)} \begin{cases} 3xV(x, y, \alpha) - \sin(\alpha)G(x, y, \alpha) - 2\cos(\alpha)F(x, y, \alpha) \\ 3yV(x, y, \alpha) - \cos(\alpha)G(x, y, \alpha) - 2\sin(\alpha)F(x, y, \alpha) \end{cases} \quad (3)$$

Where:

$$V(x, y, \alpha) = \frac{2 + (y\cos(\alpha) - x\sin(\alpha))G(x, y, \alpha)}{(1-x^2-y^2)}, \quad F(x, y, \alpha) = \frac{(x\cos(\alpha) + y\sin(\alpha))}{(1-x^2-y^2)},$$

$$G(x, y, \alpha) = \int_{\alpha}^{\alpha+\pi} \frac{dv}{(1-x\cos(v) - y\sin(v))} = \frac{\pi}{\sqrt{1-x^2-y^2}} - \frac{2}{\sqrt{1-x^2-y^2}} \tan^{-1} \left( \frac{y\cos(\alpha) - x\sin(\alpha)}{\sqrt{1-x^2-y^2}} \right) \text{ and}$$

$$\alpha = \tan^{-1} \left( \frac{y+2\dot{x}}{x-2\dot{y}} \right) - \frac{\pi}{2} \cdot \text{sign} \left( \frac{y+2\dot{x}}{x-2\dot{y}} \right) - \frac{\pi}{2} \text{sign}(y+2\dot{x})$$

The differential equation of motion is given by Eq. (4), which takes into account the hydrodynamic force  $\{Fh\}$  given in Eq. (3), the unbalance forces  $\{Fu\}$ , the rotor weight  $\{W\}$  and the generalized coordinates of the flexible rotor (with  $n$  nodes)  $\{q\}^T = \{x_1, y_1, \theta_{x1}, \theta_{y1}, \dots, x_n, y_n, \theta_{xn}, \theta_{yn}\}$ , which consider all degrees of freedom (translational and rotary displacement) of the rotating system, including the journal displacement in each bearing. If a vertical rotor is assumed, the rotor weight is not considered.

$$[M]\{\ddot{q}\} + [C]\{\dot{q}\} + [K]\{q\} = \{F_u\} + \{F_h\} - \{W\} \quad (4)$$

In order to determine the mass and stiffness matrices  $[M]$  and  $[K]$ , a finite element method is applied, to the shaft and the concentrated mass of the rotor.

The shaft damping matrix  $[C]$  contains one part that is proportional to the stiffness matrix, and the gyroscopic effects ( $[C] = \beta [K] + \Omega [G]$ ). The gyroscopic matrix is also obtained by a finite element method.

The system excitation force is due to the unbalanced mass  $m$  and its eccentricity  $e$ , expressed in Eq. (5):

$$\{F_u\} = me \begin{Bmatrix} \dots \\ \omega^2 \cos(\omega t) \\ \omega^2 \sin(\omega t) \\ \dots \end{Bmatrix} \quad (5)$$

The solution of the equation of motion is numerically obtained. In that case, the Newmark integration method was chosen, because it is a robust algorithm to solve nonlinear equations in the time domain.

In order to proceed with the simulation, a finite element model was considered. Figure 1 represents the horizontal rotor (Fig. 1.b) and its finite element model (Fig. 1.c). Node 8 corresponds to the driving-point of the non-synchronous perturbation force to be applied in order to determine the dynamic stiffness. Fig. 2 shows a waterfall plot of the system response, highlighting the fluid-induced instability and the unbalance effect in the system at critical speed.

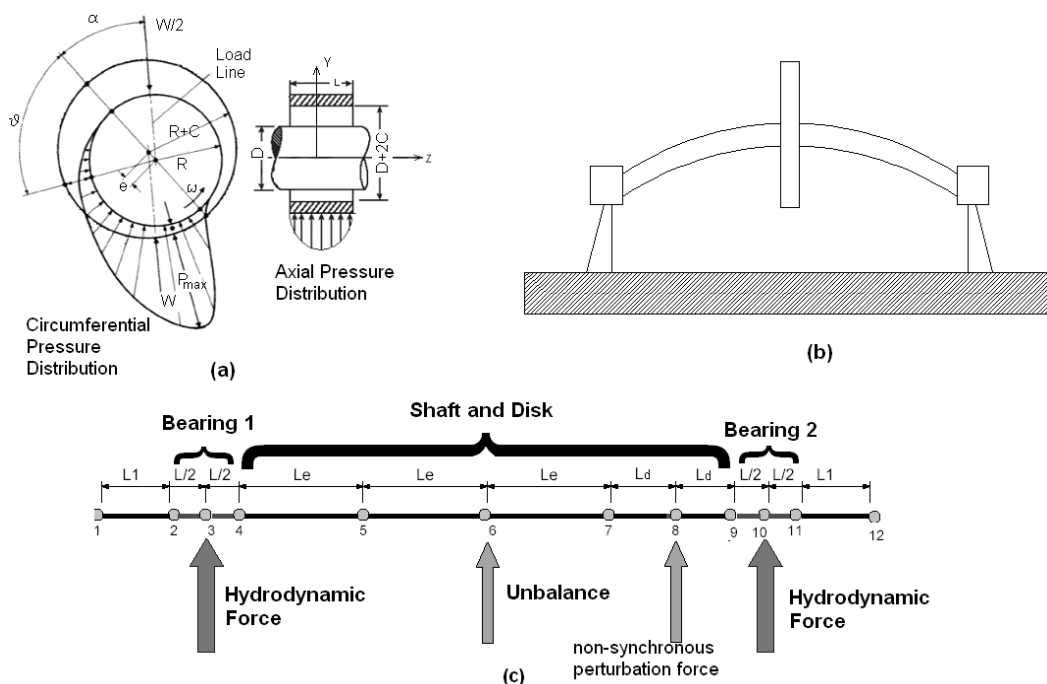


Figure 1. (a) Journal bearing scheme (b) Horizontal rotor physical model; (c) Horizontal rotor finite element model

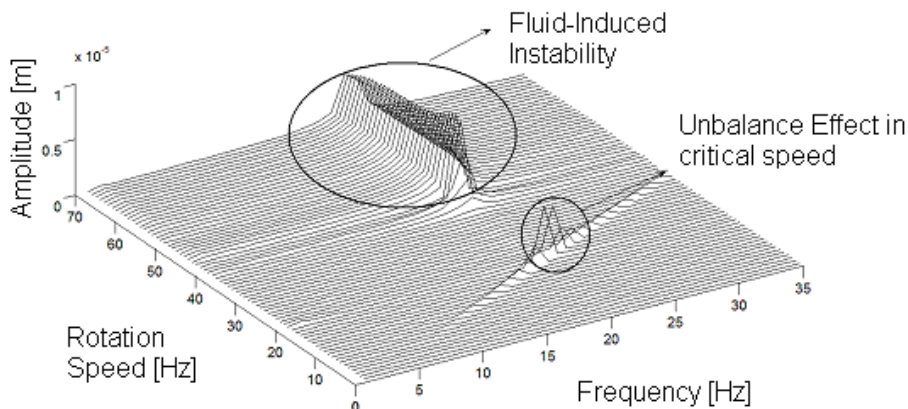


Figure 2. Waterfall plot of system response

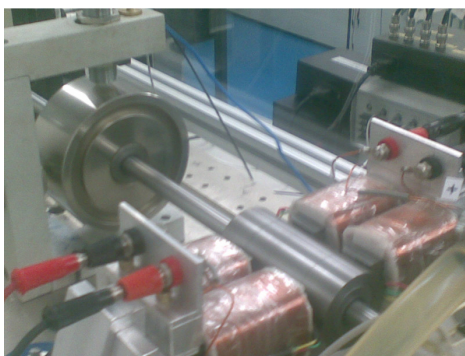
### 3. EXPERIMENTAL TEST RIG

#### 3.1 Electromagnetic actuator description

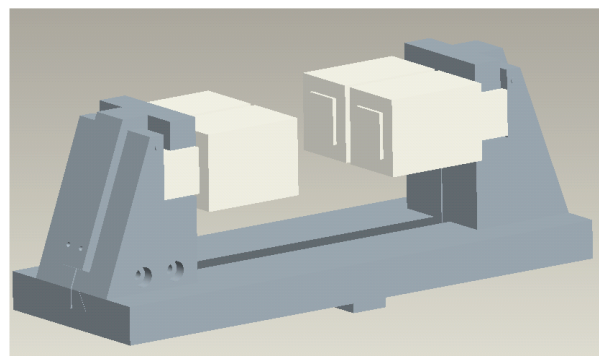
In rotordynamics, the application of electro-mechanic actuator (shaker) to accomplish excitation in rotating machinery, can cause some noise in the system response mainly in high rotational speeds, due to the friction between the actuator journal and the rotating shaft. In order to eliminate this undesired effect, it is advisable the utilization of an electromagnetic actuator, which is precisely the application of an external excitation force without contact and minimize the excessive signal noise problem when acquired in high rotational speeds.

In this context, the electromagnetic actuator appears as a possible proposal to solve this question, constituting the main focus of this work, once these devices enable the external excitation by electro-magnetic force, without any kind of mechanical contact. Such ferromagnetic forces are generated by permanent magnets or controlled electromagnets.

Castro *et al.* (2007) proposed and analysed an electro-magnetic actuator designed for application in the rotating system of the test rig. The test rig assembled is shown in Fig. 3a. A scheme of the electro-magnetic actuator and its support is presented in Fig. 3b.



(a)



(b)

Figure 3. (a) Electromagnetic actuator assembled in the test rig. (b) Electromagnetic actuator scheme

#### 3.2 Test rig description

The experimental set up consists in two hydrodynamic bearings and one unbalanced mass assembled in the shaft middle (Fig. 4), as the rotor model shown in Fig. 1c. The total length between the bearings is 600 mm. The shaft diameter is 12 mm. The concentrated mass consists of a disk of external diameter of 95 mm and length of 47 mm with mass of 2.3 kg.

A pair of cylindrical hydrodynamic bearings is used to support the shaft, which is in brass, with two different radial clearances of 90 and 125  $\mu\text{m}$ , bearing radius of 31 mm and bearing length of 20 mm. The bearings lubrication uses oil AWS 32.

The acquisition of time response to unbalance was made in the concentrated mass of the rotor. In order to obtain the curves in the horizontal and vertical directions, two magnetic proximity sensors monitor the orbit of the rotor mass.

To monitor the displacement of the shaft inside the bearings, two magnetic proximity sensors are used immersed in the oil film. Thermocouples are also assembled to measure the oil temperature, while force transducers are assembled to measure the bearing supporting forces in horizontal and vertical directions.

### 4. DYNAMIC STIFFNESS

The dynamic stiffness, which can be obtained by the ratio between the non-synchronous excitation force vector  $\vec{F}$  and the displacement (system response) vector  $\vec{R}$ , see Eq. (6), has direct relation with the phenomenon of fluid-induced vibration, generally associated with fixed geometry hydrodynamic bearings.

$$K_{DS} = \frac{\vec{F}}{\vec{R}} \quad (6)$$

The hydrodynamic force can be decomposed into two parts: a radial force, which acts in the displacement direction of the journal into the bearing, and a tangential force that acts in the fluid flow direction. Both forces are proportional to

the shaft displacement into the bearing, related to a stiffness in the radial direction, because the fluid acts as a spring in this direction, and a tangential stiffness acts in the fluid flow direction.

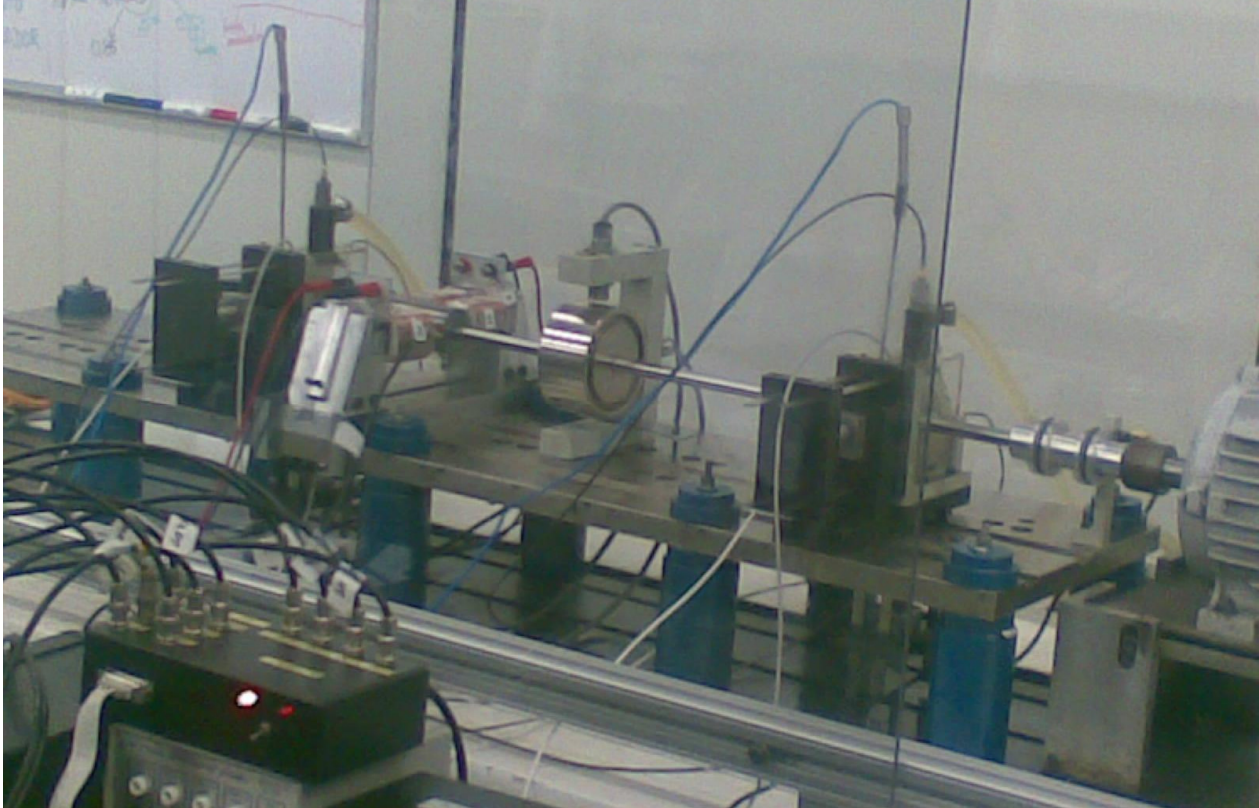


Figure 4. Complete assembly of the test bench with two hydrodynamic bearings, an inertial mass in the center and the electromagnetic actuator.

Due to the supporting hydrodynamic forces, the inertia of the rotating system and of the oil fluid damping, the shaft moves around the equilibrium position, describing an orbit. The fluid-induced instability of this rotating system depends on the relation between these parameters (radial and tangential forces, inertia of the system and viscous damping of the oil).

The dynamic stiffness constitutes, therefore, a concept that allows one to describe this relation with regard to the description of the phenomena caused by each of these parameters:

$$K_{DS} = K - M\omega^2 + jD\omega - jD\lambda\Omega = K - M\omega^2 + jD(\omega - \lambda\Omega) \quad (7)$$

Where:  $K$  is the rotor-bearing system stiffness,  $-M\omega^2$  is the mass equivalent stiffness,  $jD\omega$  is the damping equivalent stiffness and  $-jD\lambda\Omega$  is the tangential stiffness.  $M$  is the rotor mass,  $D$  is the bearing viscous damping,  $\omega$  is the whirl frequency, which can be different from the shaft rotational speed  $\Omega$ ,  $j$  is the imaginary constant, which means that the complex terms are perpendicular to the real terms, and fluid circumferential average velocity ratio  $\lambda$ .

The real part of the dynamic stiffness is the direct dynamic stiffness and the imaginary part is the quadrature dynamic stiffness. The dynamic stiffness can be related to the system response to a non-synchronous perturbation. The direct dynamic stiffness is characterized by a parabolic curve, while the quadrature dynamic stiffness by a straight line.

When the answer of the system can be obtained from a controlled perturbation, it is possible to determine the dynamic stiffness for several constant rotational speeds. Comparing the real and imaginary parts of the dynamic stiffness, the relation that indicates whether the system is stable or not is defined, or it indicates how close the system is to an instability situation.

There are some cases where the dynamic stiffness diverges from a parabolic or straight line shapes. One of the main reasons for these discrepancies is the nonlinearities (see Muszynska and Bently, 1990).

In order to obtain the dynamic stiffness, the system response needs to be filtered in the force excitation frequency. Fig. 5 shows some system responses with the filtered and non-filtered signal. In Fig. 5.a. the rotation speed is 30 Hz, so there is a frequency peak at 30 Hz, due to unbalance effect. Besides, the system vibrates at the excitation frequency (15 Hz). Due to nonlinearities the system also vibrates at 21 Hz, which is not an excited frequency. In the filtered signal, only the peak at the excitation frequency is significant. Fig. 5.b. considers the system response to the rotation speed of

30 Hz and excitation frequency of 21 Hz. In this case, only the peak at 21 Hz is noticeable. At a rotation speed of 40 Hz (Fig. 5.c.), the peak at 20 Hz is due to the fluid-induced instability, but the peak at 25 Hz (due to the excitation force) is more significant. At a rotation speed of 50 Hz (Fig. 5.d.), the fluid-induced instability at 20 Hz has a higher amplitude than the peak due to the force excitation at 25 Hz. However, this information is lost when the filtered signal is taken into account.

The dynamic stiffness of the rotor-bearing system at a rotation speed of 30 Hz is shown in Fig. 6. Fig 6.a. shows the dynamic stiffness neglecting the nonlinearities, while Fig. 6.b. considers these nonlinearities. In both cases the direct dynamic stiffness is a parabolic curve, which is in accordance with Eq. (7). However, the quadrature dynamic stiffness for the case where the nonlinearities are taken into account has a different behaviour from Eq. (7) (a straight line). For both cases the quadrature dynamic stiffness is zero for excitation frequency close to 15 Hz, showing that the margin of stability is close to 6 Hz (difference between the excitation frequencies where direct and quadrature dynamic stiffness are zero). Therefore, the consideration of nonlinearities does not have significant influence on the threshold of stability. The evolution of this margin can be observed on Fig. 7. At a rotation speed of 35 Hz (Fig. 7.a.), the quadrature dynamic stiffness is zero close to 18 Hz. As the direct dynamic stiffness is still zero at 21 Hz, the margin of stability is 3 Hz. At a higher rotation speed the precession motion due to fluid-induced instability is predominant (see Fig. 2) and the dynamic stiffness does not have the characteristic of Eq. (7), as can be seen in Fig. 8, where the rotation speed is 50 Hz. When the rotation speed is 40 Hz, the margin of stability is close to 1 Hz (see Fig 7.b), and the system motion is sub-synchronous. At a higher rotation speed the precession motion due to fluid-induced instability is predominant (see Fig. 2) and the dynamic stiffness does not have the characteristic of Eq. (7), as can be seen in Fig. 8, where the rotation speed is 50 Hz.

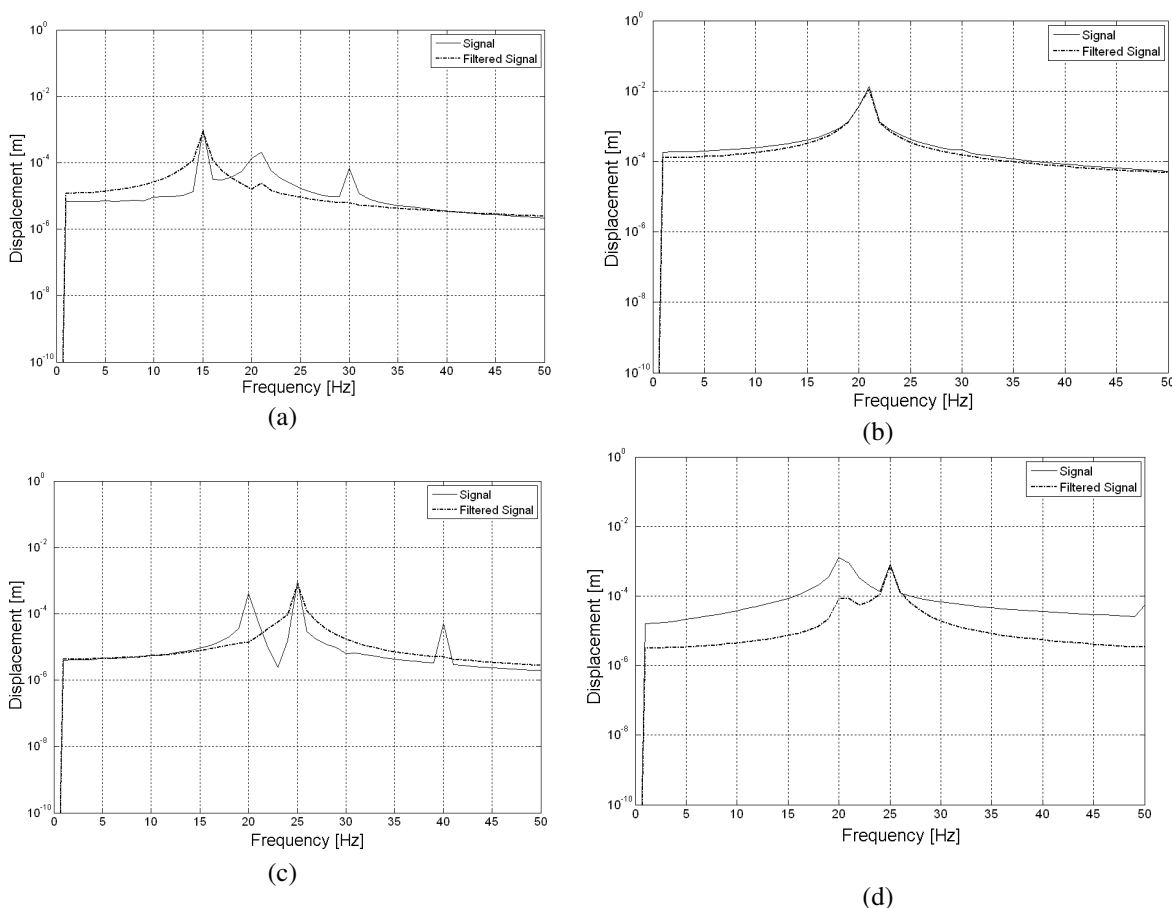


Figure 5. Response FFT (a) Rotation speed of 30 Hz and excitation frequency of 15 Hz; (b) Rotation speed of 30 Hz and excitation frequency of 21 Hz; (c) Rotation speed of 40 Hz and excitation frequency of 25 Hz; (d) rotation speed of 50 Hz and excitation frequency of 25 Hz

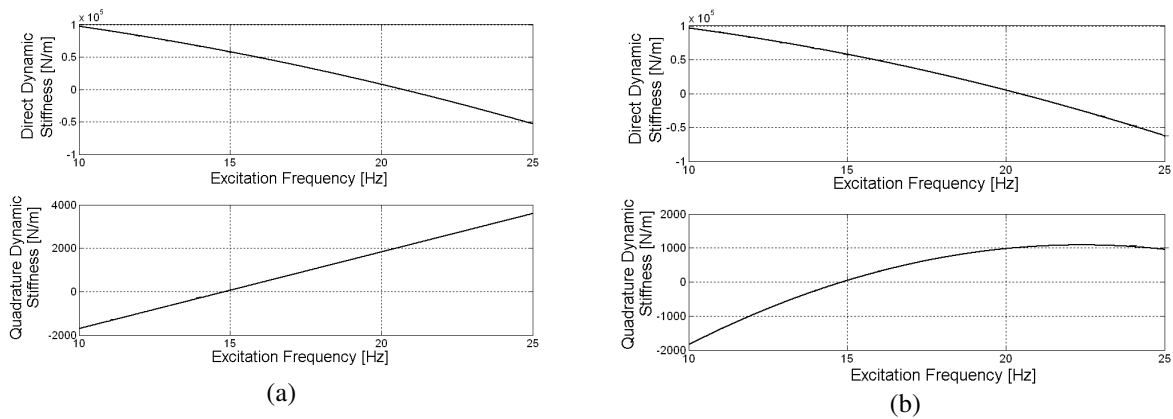


Figure 6. Dynamic stiffness for rotation speed of 30 Hz (a) Neglecting nonlinearities; (b) Considering nonlinearities

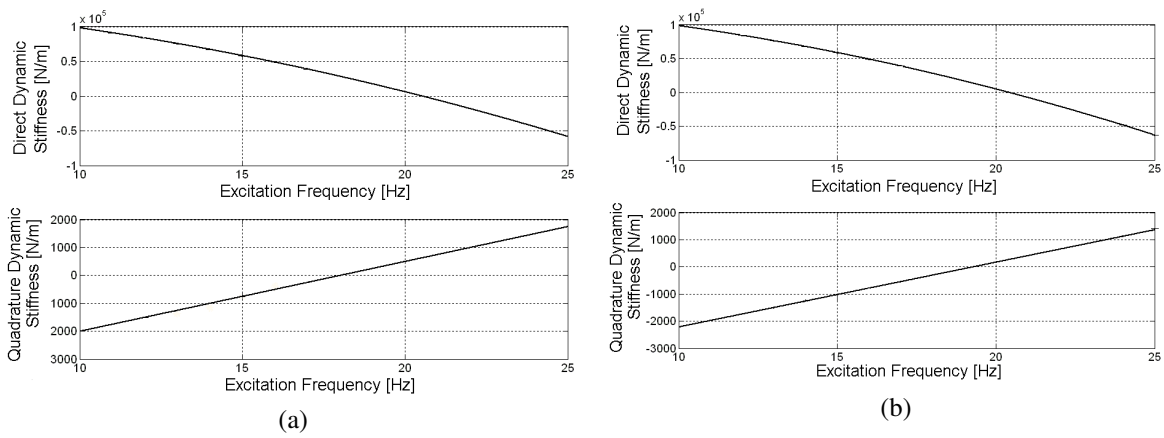


Figure 7. Dynamic stiffness for rotation speed neglecting nonlinearities; (a) Rotation speed of 35 Hz; (b) Rotation speed of 40 Hz.

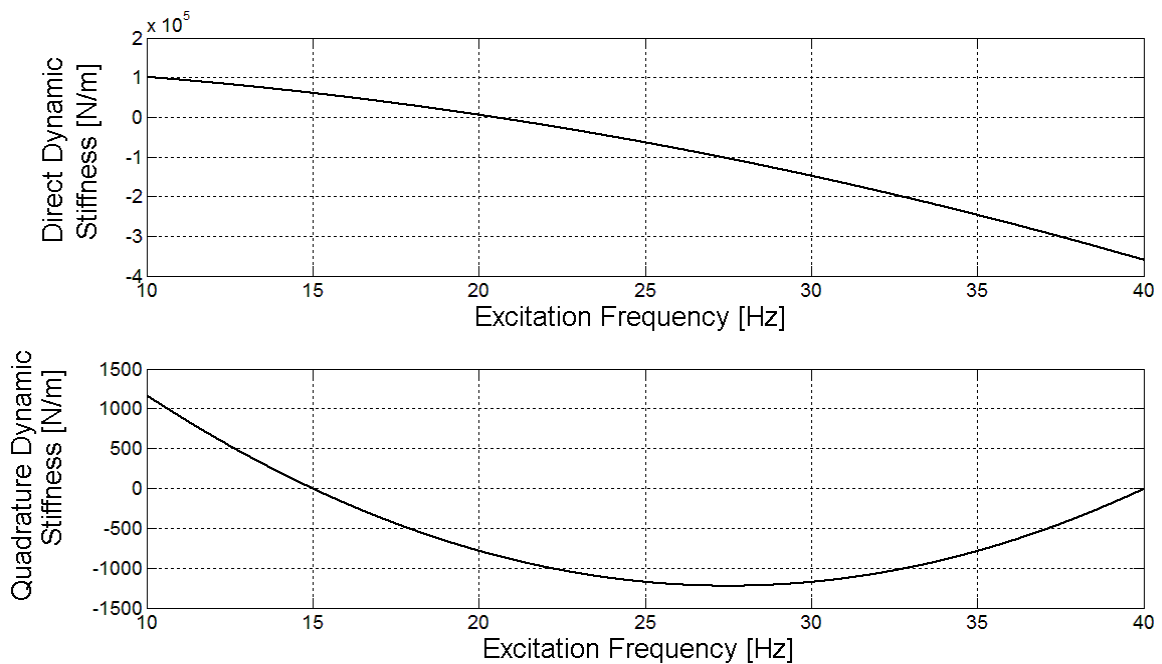


Figure 8. Dynamic stiffness for rotation speed considering nonlinearities for rotation speed of 50 Hz

Experimental tests were accomplished to determine the dynamic stiffness of the rotor-bearing system in the test rig, through a non-synchronous excitation from the electromagnetic actuator. The rotation speed chosen for these tests were 30 and 35 Hz (Figs. 9 and 10), because they allow the determination of how the system response approaches the threshold of instability when the rotation speed increases.

Some nonlinearity is observed in the imaginary part of the dynamic stiffness, because its curve does not approach to a straight line, but to a parabolic curve. That means that the imaginary part of the dynamic stiffness, which has a linear relation to the excitation frequency  $\omega$  in Eq. (7), has a parabolic relation to the excitation frequency.

Besides, the imaginary part is zero at 8 Hz for a rotation speed of 30 Hz, 11 Hz for 35 Hz and 14 Hz for 45 Hz. In doing so, fluid circumferential average velocity ratio  $\lambda$  is respectively 0.27, 0.31 and 0.31. Usually, the value of this ratio is close to 0.5. However, this discrepancy can be caused by the eccentricity inside the bearing, as shown by Muszynska (1995) and Jordan (2000). The fluid circumferential average velocity ratio  $\lambda$  decreases with the eccentricity increasing until occurs a collapse for higher eccentricities. In that case, there are some unknown bearing loads, due to residual misalignment or shaft bow. These loads can be the source of a higher eccentricity. On the other hand, another possible case for this discrepancy is the effect of the application of the electromagnetic actuator, which introduces some stiffness in the system.

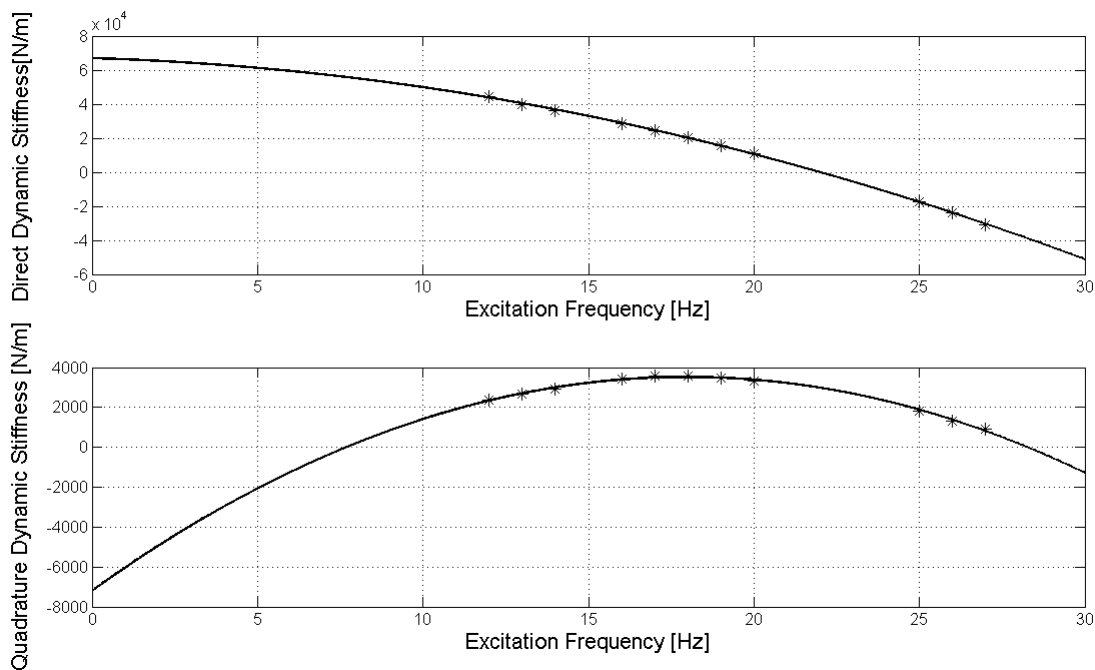


Figure 9. Dynamic stiffness of the experimental test rig for a rotation speed of 30 Hz

## 5. CONCLUSIONS

A model of rotor-bearing system is proposed, considering nonlinear hydrodynamic forces. The shaft and disk of the rotor are modelled by finite element model. The horizontal rotor was simulated.

In order to determine the dynamic stiffness, the system response filtered in the frequency of the excitation force was used. However, if the rotor-bearing system is in an instable motion, the main frequency is due to the self-excitation caused by the hydrodynamic journal bearing.

The dynamic stiffness was estimated through the simulation of a non-synchronous perturbation in the nonlinear rotor-bearing system. The dynamic stiffness nonlinearities have an important part in the dynamic stiffness behaviour, but they do not influence the system margin of stability.

Therefore, it seems that the dynamic stiffness can also be used to determine the threshold of stability in a nonlinear rotor-bearing system.

Besides, all simulations showed that the margin of stability steadily decreases as the rotor speed approaches the threshold of stability.

The same procedure was adopted to determine the dynamic stiffness of the test rig. However, the fluid circumferential average velocity ratio  $\lambda$  presented different values from those obtained in the simulation. Two possible reasons for this discrepancy can be the high shaft eccentricity inside the bearing or the application of the electromagnetic actuator. The first possibility is caused by other excitation source, as a residual misalignment caused by the coupling between the driven motor and the rotor. The second one introduces stiffness to the system, which decreases

the instability of the system, see Jordan (2000). In future works, the cause of the difference between the simulated and experimental fluid circumferential average velocity  $\lambda$  will be investigate, through a monitoring of the shaft eccentricity and the effect of the electromagnetic force variation.

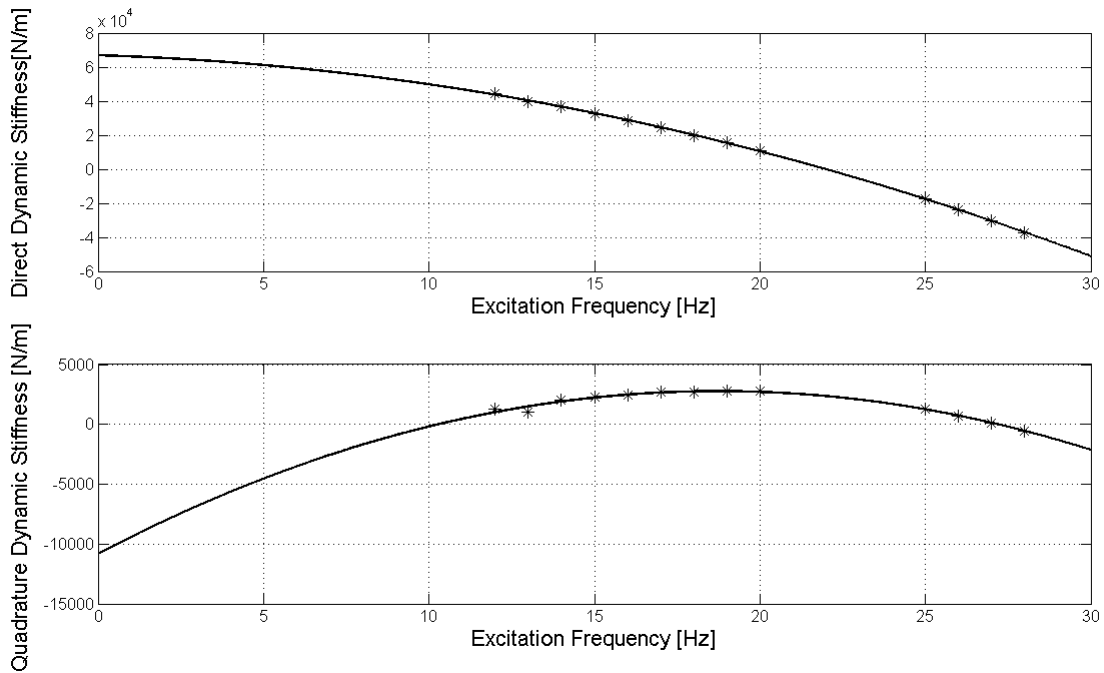


Figure 10. Dynamic stiffness of the experimental test rig for a rotation speed of 35 Hz

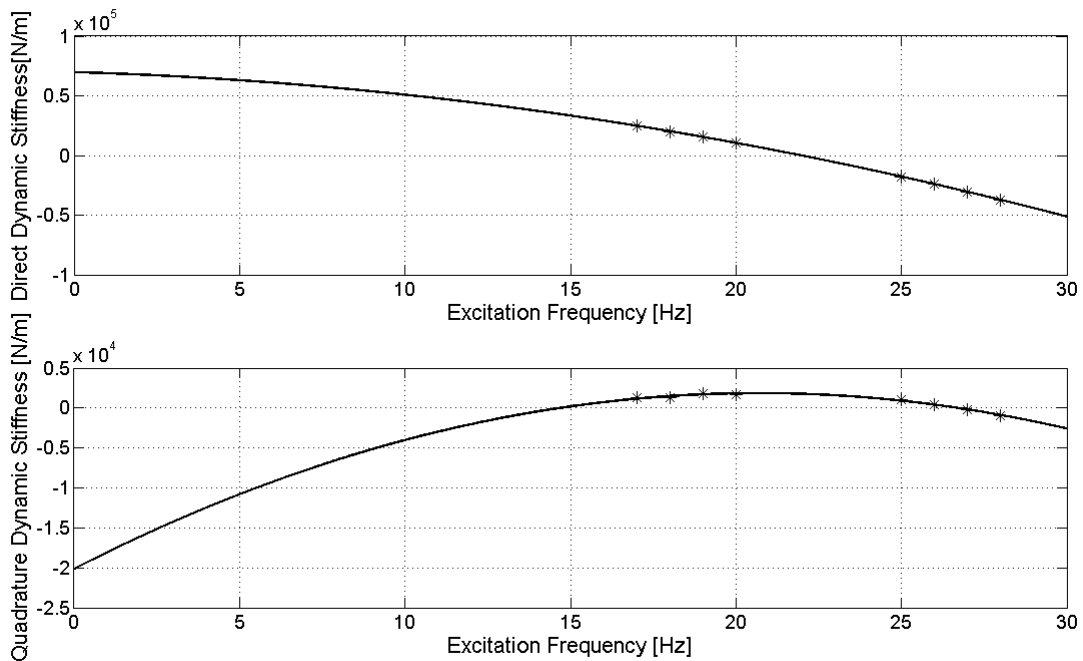


Figure 11. Dynamic stiffness of the experimental test rig for a rotation speed of 45 Hz

## 6. ACKNOWLEDGEMENTS

The authors thank FAPESP, CNPq and CAPES for the support to this research.

## 7. REFERENCES

- Archer, J. S. , 1965, "Consistent Matrix Formulations for Structural Analysis Using Finite-Element Techniques", AIAA Journal, Vol. 3, n. 10, pp. 1910-1918.
- Bently, D. E., Hatch, C., Jesse, R., Whiteley, J., "Dynamic Stiffness in whirl and whip", Orbit, first quarter, 1998, pp. 4-9.
- Capone, G., 1986, "Orbital motions of rigid symmetric rotor supported on journal bearings", La Meccanica Italiana, Vol. 199, pp. 37-46.
- Capone, G., 1991, "Descrizione analitica del campo di forze fluidodinamico nei cuscinetti cilindrici lubrificati", L'Energia Elettrica, Vol. 3, pp. 105-110.
- Castro, H F, Cavalca K L, Nordmann R., 2006, "Rotor-bearing system instabilities considering a non-linear hydrodynamic model", 7th IFToMM - Conference on Rotor Dynamics, Vienna, Austria, paper ID-136, pp. 1-10.
- Castro, H F, Cavalca K L, Nordmann R., 2008, "Whirl and whip instabilities in rotor-bearing system considering a nonlinear force model", Journal of Sound and Vibration, n. 317, pp. 273-293.
- Castro, F. F., Furtado, R. M., Cavalca, K. L., Pederiva, R., Butzek, N., Nordmann, R. "Experimental Performance Evaluation of Magnetic Actuator used in Rotating Machinery Analysis". Journal of the Brazilian Society of Mechanical Sciences, ABCM – Rio de Janeiro, v. 29 n. 1, 2007, pp. 1-10.
- Childs, D., 1993, "Turbomachinery Rotordynamics". Wiley-Intersciences, New York.
- Crandall, S., 1990, "Form Whirl to Whip in Rotordynamics", Transactions of IFToMM 3rd International Conference on Rotordynamics, Lyon, France, pp. 19-26.
- Gasch, R., Nordmann, R., Pfützner, H., 2002, "Rotordynamik". Springer, Berlin, 705 p.
- Jordan, M. A., 2000, "Experimental Results and Implications of Perturbation Testing with ServoFluid™ Control Bearings", Orbit, second quarter, 2000, pp. 10-17.
- Lund, J. W., Saibel, E., 1967, "Oil whip whirl orbits of a rotor in sleeve bearings", ASME Journal of Engineering for Industry. n. 89, pp. 813-823.
- Muszynska, A., 1986, "Whirl and Whip – Rotor Bearing Stability Problems", Journal of Sound and Vibration, Vol. 110 n. 3, pp. 443-462.
- Muszynska, A., 1988, "Stability of Whirl and Whip in Rotor Bearing System", Journal of Sound and Vibration. Vol. 127 n. 1, pp. 49-64.
- Muszynska, A., Bently, D. E., 1989, "Fluid-Generated Instabilities of rotors", Orbit, Vol. 10, n. 1, pp. 6-14.
- Muszynska, A., Bently, D. E., 1990, "Frequency-swept rotating input perturbation techniques and identification of the fluid force models in rotor/bearing/seal systems and fluid handling machines", Journal of Sound and Vibration, Vol. 143 n. 1, pp. 103-124.
- Muszynska, A. , 1995, "Modal Testing of Rotors with Fluid Interactions". International Journal of Rotating Machinery, v. 1, n. 2, pp. 83-116.
- Nelson, H. D., McVaugh, J. M., 1976, "Dynamics of Rotor-Bearing Systems Using Finite Elements", ASME Journal of Engineering for Industry, Vol. 98, pp. 593-600.
- Newkirk, B. L., and Taylor, H. D, 1924, "Shaft Whipping", General Electric Review, Vol. 27, n. 3, pp. 169-178.
- Newkirk, B. L., and Taylor, H. D., 1925, "Shaft Whipping due to Oil Action in Journal Bearings", General Electric Review, Vol. 28, n. 8, pp. 559-568.
- Reynolds, O., 1886, "On the Theory of Lubrication and its Application to Mr. Beauchamp Tower's Experiments, including an Experimental Determination of the Viscosity of Olive Oil", Philosophical Transactions of Royal Society of London, Series A, Vol. 177, Part 1, pp.157-234.
- Ruhl, R. L., Booker J. F., 1972, "A Finite Element Model for Distributed Parameter Turborotor Systems", ASME Journal of Engineering for Industry, Vol. 94, pp.128-132.

## 8. RESPONSIBILITY NOTICE

The authors are the only responsible for the printed material included in this paper.